J Low Temp Phys
DOI 10.1007/s10909-016-1718-2

Coupled Dynamics for Superfluid ^{4}He in a Channel

D. Khomenko[1] · **P. Mishra** [1] · **A. Pomyalov**[1]

Received: 19 July 2016 / Accepted: 21 November 2016

Abstract We study the coupled dynamics of normal and superfluid components of superfluid ^{4}He in a channel considering the counterflow turbulence with laminar normal component. In particular, we calculated profiles of the normal velocity, the mutual friction, the vortex line density and other flow properties and compared them to the case where the dynamic of the normal component is "frozen." We have found that the coupling between the normal and superfluid components leads to flattening of the normal velocity profile, increasingly more pronounced with temperature, as the mutual friction, and therefore, coupling becomes stronger. The commonly measured flow properties also change when the coupling between the two components is taken into account.

Keywords Superfluid helium · Coupled dynamics · Thermal counterflow

1 Introduction

Superfluid ^{4}He below transition temperature $T_\lambda \simeq 2.17\,\mathrm{K}$ may be viewed as a two-fluid system [1–3] consisting of a normal fluid with very low kinematic viscosity $\nu_\mathrm{n}(T)$ and an inviscid superfluid component that have their own densities, $\rho_\mathrm{n}(T)$, $\rho_\mathrm{s}(T)$, and velocity fields, $\boldsymbol{u}_\mathrm{n}(\boldsymbol{r},t)$, $\boldsymbol{u}_\mathrm{s}(\boldsymbol{r},t)$. Due to quantum mechanical restriction, the circulation around the superfluid vortices is equal to $\kappa = h/m \simeq 10^{-3}\,\mathrm{cm}^2/\mathrm{s}$, where h is the Plank constant and m denotes the mass of a ^{4}He atom. The singly quantized vortices usually arrange themselves in a tangle, referred to as *quantum turbulence*, that may

✉ D. Khomenko
dmytro.khomenko@weizmann.ac.il

[1] Department of Chemical Physics, Weizmann Institute of Science, 76100 Rehovot, Israel

Published online: 29 November 2016

be characterized by a vortex line density (VLD) $\mathcal{L}$, i.e., total length of the quantized vortex line in a unit volume [4,5].

The large-scale motion of such a system may be described by the Hall–Vinen–Bekarevich–Khalatnikov equations (HVBK) [6,7], where both components are considered as continuous fluids, coupled by a mutual friction force. The microscopic description of the vortex lines dynamics at scales that are still much larger than the vortex core size $a_0 \approx 10^{-8}$ cm was proposed by Schwarz [8,9] in the framework of the vortex filament method (VFM). In his approach, the influence of the normal component on the dynamics of the quantum vortex lines is accounted through the mutual friction force with the predefined time-independent normal fluid velocity. It was soon realized that the back-reaction of the vortex tangle on the dynamics of the normal component may be important and several self-consistent methods, coupling the Navier–Stokes equation for the normal component with the Lagrangian description of the vortex lines dynamics, were proposed [10–12]. These methods are computationally challenging, given the wide range of scales involved in the problem. Such self-consistent studies were limited to space-homogeneous flows with diluted vortex tangles.

The VFM methods were extended to the wall-bounded flows, firstly in the local induction approximation [13,14] and more recently included full Biot–Savart description of the tangle [15–18]. Also here, a time-independent mean normal velocity profile or a snapshot of the turbulent velocity field was imposed to generate the quantum vortex tangle.

Depending on the way the quantum turbulence is generated in the channel or pipe, the normal and superfluid components flow in the same direction or in the opposite directions. In the latter case (the thermal counterflow), a relative, counterflow velocity V_{ns} is established in the channel. At sufficiently large values of V_{ns}, the quantum vortex tangle is created. As V_{ns} increases, the thermal counterflow passes several stages. At relatively low values of counterflow velocity, the normal component remains laminar, while a fully developed quantum vortex tangle is formed, indicating superfluid turbulence. This regime was labeled as T1 state [19]. At higher values of V_{ns}, the normal component also becomes turbulent, forming the so-called T2 state. Recently, coupled profiles of the laminar normal and the superfluid velocities in a two-dimensional planar channel were calculated using the Navier–Stokes description for the normal component [20].

In this paper, we address the back-reaction of the quantum vortex tangle on the normal velocity profile, restricting our study to the T1 state of the counterflow in the three-dimensional planar channel. Here we describe the laminar normal velocity by its mean profile (neglecting normal velocity fluctuations), but allow its evolution, driven by the mutual friction force that couples the dynamics of the mean normal velocity with the evolution of the vortex tangle. To be consistent with the nature of the mean profile, the mutual friction force, generated by the vortex tangle, is integrated over space and short intervals of time. Such a multi-scale, multi-time approach allows us to follow the coupled dynamics of the two components and to account for the influence of the vortex tangle on the normal component.

We have found that the initially parabolic mean normal velocity profile evolves to a flatter shape, with effect stronger for higher temperature and counterflow velocities.

As a consequence, the VLD profile becomes more uniform in the channel core with the peaks pushed toward the wall. Both the global and microscopic properties of the flow change compared to the uncoupled dynamics, although this effect is significant only at high temperatures.

2 Coupled System

In the framework of the two-fluid description of superfluid ^{4}He, the dynamics of the normal component is given by the HVBK equations [6,7,10]:

$$\frac{\partial \boldsymbol{u}_\mathrm{n}}{\partial t} + (\boldsymbol{u}_\mathrm{n} \cdot \nabla)\, \boldsymbol{u}_\mathrm{n} = \frac{\nabla P}{\rho_\mathrm{n}} + \frac{\boldsymbol{F}_\mathrm{ns}}{\rho_\mathrm{n}} + \nu_\mathrm{n} \Delta \boldsymbol{u}_\mathrm{n}, \tag{1}$$

where the mutual friction force $\boldsymbol{F}_\mathrm{ns}$ couples the two components and the effective pressure P is defined by: $\nabla P = -(\rho_\mathrm{n}/\rho)\, \nabla p + \rho_\mathrm{s} S \nabla T$ (S is the entropy and $\rho = \rho_\mathrm{n} + \rho_\mathrm{s}$ is the density of helium II). For the laminar flow in the channel, Eq. (1) simplifies to an equation for the mean normal velocity:

$$\frac{\partial V_\mathrm{n}(y)}{\partial t} = \frac{dP}{dx} + \frac{\mathcal{F}_\mathrm{ns}(y)}{\rho_\mathrm{n}} + \nu_\mathrm{n} \frac{\partial^2 V_n(y)}{\partial y^2}, \tag{2}$$

Here we took into account that in the planar channel geometry the normal velocity field $V_\mathrm{n}(y)$ depends on the wall-normal direction only and has only one nonzero (streamwise) component along channel. A streamwise projection $\mathcal{F}_\mathrm{ns}(y)$ of the mutual friction force,

$$\boldsymbol{F}_\mathrm{ns} = \frac{\rho_s}{\Omega} \int_{\mathcal{C}'} (\alpha \boldsymbol{s}' \times [\boldsymbol{s}' \times \boldsymbol{V}_\mathrm{ns}] + \alpha' \boldsymbol{s}' \times \boldsymbol{V}_\mathrm{ns}) d\xi, \tag{3}$$

is defined by the dynamics of the quantum vortex tangle [9]. Here $\boldsymbol{s}$ is a radius vector to the points on the vortex line, $'$ denotes the derivative along the vortex line, and α, α' are the mutual friction coefficients. The integral in Eq. (3) is taken along the vortex lines $\mathcal{C}'$, residing inside a suitably defined coarse-grained volume Ω.

The instantaneous counterflow velocity $\boldsymbol{V}_\mathrm{ns} = \boldsymbol{V}_\mathrm{n} - \boldsymbol{V}_\mathrm{s}$ is defined by velocities of the normal and superfluid components. The superfluid velocity $\boldsymbol{V}_\mathrm{s} = V_\mathrm{s}^0 + \boldsymbol{V}_\mathrm{BS}(\boldsymbol{s})$ contains contributions of the vortex tangle velocity $\boldsymbol{V}_\mathrm{BS}(\boldsymbol{s})$ in the Biot–Savart representation, integrated over the entire vortex configuration $\mathcal{C}$ and the applied superfluid velocity V_s^0, defined by the counterflow condition $\rho_\mathrm{n} \langle \boldsymbol{V}_\mathrm{n} \rangle_v + \rho_\mathrm{s} \langle \boldsymbol{V}_\mathrm{s} \rangle_v = 0$. Here $\langle \ldots \rangle_v$ stands for global volume averaging.

Implementation Details The simulations were set up in a planar channel of the size $4h \times 2h \times 2h$, $h = 0.05$ cm. The vortex line dynamics was solved using VFM [9,18,21] with fourth-order difference scheme for the derivatives $\boldsymbol{s}'$ and $\boldsymbol{s}''$ [22,23]. We used the periodic boundary conditions in the streamwise(x) and the spanwise(z) directions, with slip conditions in the wall-normal y direction, the line resolution $\Delta\xi_0 = 0.0016$

Table 1 Parameters of helium II, used in simulations [24]

T (K)	α	α'	$\rho_n\,(\mathrm{g/cm^3})$	ρ_n/ρ_s	$\nu = \eta/\rho_n\,(\mathrm{cm^2/s})$
1.45	6.1×10^{-2}	1.8×10^{-2}	1.3×10^{-2}	1.0×10^{-1}	1.0×10^{-3}
1.6	9.7×10^{-2}	1.6×10^{-2}	2.4×10^{-2}	1.9×10^{-1}	5.6×10^{-4}
1.9	2.1×10^{-1}	8.3×10^{-2}	6.1×10^{-2}	7.2×10^{-1}	2.2×10^{-4}

cm and the time step δt_s, defined by the stability condition of the fourth-order Runge-Kutta scheme. The dynamics of the mean normal velocity profile $V_\mathrm{n}(y, t)$, Eq. (2), was solved using second-order finite-difference scheme for the viscous term, second-order Adams-Bashforth method for the time marching and no-slip conditions on the solid walls. The effective pressure gradient $P_\mathrm{x} = \mathrm{d}P/\mathrm{d}x$ was used as a free parameter of the system.

To calculate the mutual friction term, we used a two-stage approach. The term $\mathcal{F}_\mathrm{ns}$ in Eq. (2) implies averaging over space and time, while the term F_ns is instantaneous and is averaged only over space. The parabolic normal velocity profile was initiated on a grid of a mesh size $\delta y = 0.00625$ cm in the wall-normal direction. Using this profile, the superfluid system was propagated for $\Delta t = 10\delta t_\mathrm{s}$. At each time step, the mutual friction force F_ns was integrated over thin slices of volume $4h \times \delta y \times 2h$ and then averaged during Δt. The resulting values of $\mathcal{F}_\mathrm{ns}$ were assigned to the middle points of the slices in the y-direction and linearly interpolated to the normal velocity grid points. With this mean mutual friction force, $V_\mathrm{n}(y)$ was then propagated over the time interval of Δt using the same δt_s. The newly obtained values of $V_\mathrm{n}(y)$ were interpolated to the positions of the line points for the next cycle of the superfluid dynamics, during which V_n was considered constant.

The resulting profiles of $\mathcal{L}(y)$, $V_\mathrm{s,n}(y)$ and other related properties were obtained by integrating over the same slices as the mutual friction, assigned to the middle points of the slices and then averaged over more than 50 steady-state configurations. The simulations were carried out for $T = 1.45$, 1.6 and 1.9 K and a number of P_x values. The material properties of the fluid components [24] are given in Table 1. Notice that we did not use the modified mutual friction coefficients [11], because we only consider the mean normal velocity field.

3 Results and Discussion

The steady-state profiles of $V_\mathrm{n}(y)$ as a function of the normalized wall-normal coordinate $y^\dagger = y/h$ for different T and values of the effective pressure are shown in Fig. 1. To compare the shapes of the profiles, we normalized them by $3/2\ \langle V_\mathrm{n}\rangle$. For the original parabolic normal velocity profile, this value corresponds to the centerline velocity. For modified profiles, this relation is no longer valid. The profiles of $V_\mathrm{n}(y)$ become flatter in the center of the channel, increasingly so with increasing temperature and applied pressure gradient.

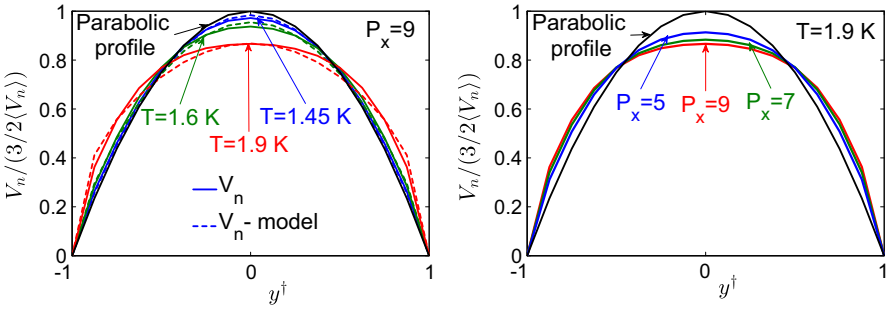

Fig. 1 Comparison of the normalized velocity profiles $V_{\rm n}(y)/(3/2\,\langle V_{\rm n}\rangle)$ versus $y^\dagger = y/h$, $y^\dagger \in [-1, 1]$ for the effective pressure gradient $P_{\rm x} = 9$ and different temperatures (*left panel*) and for $T = 1.9\,{\rm K}$ and different values of $P_{\rm x}$ (*right panel*). The normalized parabolic profile is shown by a *black solid line*. In the *left panel*, we also show the model profiles Eq. (8)(*dashed lines*) for $T = 1.45\,{\rm K}$ [$\langle V_{\rm n}\rangle = 1.22\,{\rm cm/s}$], 1.6 [$\langle V_{\rm n}\rangle = 1.01\,{\rm cm/s}$] and $1.9\,{\rm K}$ [$\langle V_{\rm n}\rangle = 0.69\,{\rm cm/s}$] (Color figure online)

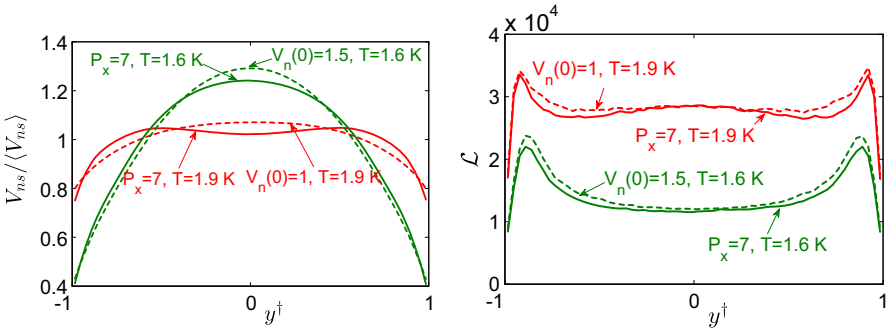

Fig. 2 Comparison of the normalized $V_{\rm ns}$ (*left*) and VLD profiles (*right*) for the coupled dynamics (*solid lines*) and for the time-independent parabolic $V_{\rm n}$ (*dashed lines*) for $T = 1.6$ and $1.9\,{\rm K}$ (Color figure online)

These profiles exhibit a different kind of flattening than the velocity profiles recently visualized by Marakov et al. [25] for the experimental conditions close to the laminar–turbulent transition in the normal component. Our strictly laminar model does not reproduce these conditions. The change in the numerical superfluid velocity profile shape is solely due to the interaction with the normal components.

The resulting profile of the counterflow velocity $V_{\rm ns}(y)$ is shown by solid lines in Fig. 2, left panel, for $T = 1.6$ and $1.9\,{\rm K}$, together with profiles, obtained using a time-independent parabolic normal velocity profile with similar $\langle V_{\rm n}\rangle$ (dashed lines). The flatter profiles of $V_{\rm n}$ lead to a change in the profiles of $V_{\rm ns}$, especially in the channel core. The vortex lines tend to concentrate in the regions with smaller $V_{\rm n}$[18], such that the peaks in the VLD profiles, shown in Fig. 2, right panel, are pushed further toward the walls. The statistical properties of the vortex tangle are commonly characterized by a relation between mean VLD in the channel and $\langle V_{\rm ns}\rangle$: $\langle\mathcal{L}\rangle^{1/2} = \gamma(T)(\langle V_{ns}\rangle - v_0)$, where $\gamma(T)$ is a temperature-dependent coefficient and v_0 is a virtual origin. This relation is valid only globally [26]. We compare in Table 2 the values of γ, obtained with different profiles. Notice that the results for different profiles at temperatures

Table 2 Values of $\gamma(T)$ for different profiles: γ_c for the coupled dynamics, γ_p for the frozen parabolic profile

T (K)	γ_c(s/cm^2)	γ_p(s/cm^2)	γ_p(s/cm^2) [16]	γ_{hp}(s/cm^2) [17]	γ_{uni}(s/cm^2) [21]
1.3	–	–	67.9	31	72.1
1.45	83	85	–	–	–
1.6	114	113	83.6	47	115.7
1.9	165	144	105.7	103	148

For comparison, we give also values for the parabolic profile, Ref. [16], the Hagen–Poiseuille profile γ_{hp} [17] and for the uniform normal velocity γ_{uni} [21]

$T = 1.45$ and 1.6 K are close, while for higher $T = 1.9$ K, γ_c is significantly larger than γ_p. The values of γ_p are close to those of uniform V_n for all temperatures. Notably, our results are higher than those obtained in Refs. [16,17] for the channel counterflow with the parabolic and Hagen–Poiseuille profiles. This discrepancy may stem from the fact that in both [16,17] the counterflow condition did not include the contribution from the vortex tangle, which is not negligible for dense tangles.

Model profile of V_n To rationalize the observed modifications of the normal velocity profile, we notice that in the steady state the mutual friction force is almost constant across the channel, except for the near-wall region, where it quickly falls to zero. Therefore, qualitatively, the mutual friction redefines the effective pressure gradient in the middle of the channel $P_x + \langle \mathcal{F}_{ns} \rangle / \rho_n$, while near the wall it remains P_x. Such a change leads to the flattening of the normal velocity profile (as compared to the classic parabolic profile).

To find the new, flattened, V_n, we first model the shape of the mutual friction force profile by a function:

$$\mathcal{F}_{ns} = -\left(1 - y^{\dagger n}\right) \mathcal{F}_{ns}(0), \tag{4}$$

where n is an even integer and $\mathcal{F}_{ns}(0)$ is the mutual friction force in the middle of the channel. To account for the sharp transition from almost a constant value in the middle of the channel to zero at the wall, large values of n are required. In this work, we use $n = 14$. Substituting (4) into the steady-state equation (2) for V_n, we obtain:

$$\frac{\nu}{h^2} \frac{d^2 V_n}{d y^{\dagger 2}} = -P_x + \frac{\mathcal{F}_{ns}(0)}{\rho_n} \left(1 - y^{\dagger n}\right). \tag{5}$$

This equation is easily solved, giving:

$$V_n\left(y^\dagger\right) = A\left(1 - y^{\dagger 2}\right)\left[1 + \frac{2C}{(n+2)(n+1)} \frac{1 - y^{\dagger n+2}}{1 - y^{\dagger 2}}\right],$$
$$A = h^2 P_{x,m}/(2\nu)\,,\; C = \mathcal{F}_{ns}(0)/(\rho_n P_{x,m})\,,\; P_{x,m} = P_x - \mathcal{F}_{ns}(0)/\rho_n\,. \tag{6}$$

Notice that when the mutual force is not taken into account so that $\mathcal{F}_{\rm ns}(0) = 0$, the profile (6) reduces to the classical parabolic profile. To proceed, we notice that $\langle V_n \rangle = 2A/3 + 2AC/[(n+1)(n+3)]$ and $\langle \mathcal{F}_{\rm ns} \rangle = n\mathcal{F}_{\rm ns}(0)/(n+1)$. Using the counterflow condition and the Gorter–Mellink relation [27] between the mean mutual friction force and $\langle V_{\rm ns} \rangle$, we find

$$\langle \mathcal{F}_{\rm ns} \rangle = A_{\rm GM}\rho_{\rm s}\rho_{\rm n}(1+\rho_{\rm n}/\rho_{\rm s})^3\langle V_{\rm n}\rangle^3 \equiv \frac{\rho_n \nu}{h^2}\frac{\langle V_n\rangle^3}{V_0^2}\,. \tag{7}$$

The characteristic velocity $V_0 = \left(A_{\rm GM}\rho_s h^2(1+\rho_{\rm n}/\rho_{\rm s})^3/\nu\right)^{-1/2}$ corresponds to a balance between the mutual friction and viscous terms, and $A_{\rm GM}$ is the Gorter–Mellink constant. Combining all above, we finally obtain:

$$V_{\rm n}\left(y^\dagger\right) = \frac{3}{2}\langle V_{\rm n}\rangle\left[V_1\left(1-y^{\dagger 2}\right) + V_2\left(1-y^{\dagger n+2}\right)\right], \tag{8}$$

where $V_1 = \left(1 - \frac{1}{n(n+3)}\left[\frac{\langle V_{\rm n}\rangle}{V_0}\right]^2\right)$ and $V_2 = \frac{2}{3(n+2)n}\left[\frac{\langle V_{\rm n}\rangle}{V_0}\right]^2$ are the T-dependent expansion coefficients. The model profiles are compared with the numerical results in Fig. 1, left panel. These profiles were calculated using $n = 14$ and the following values of the Gorter–Mellink constant $A_{\rm GM}$, calculated from the mutual friction force in the coupled dynamics: $A_{\rm GM}(1.45) = 20.7\,{\rm cm}\cdot{\rm s/g}$, $A_{\rm GM}(1.6) = 35.7\,{\rm cm}\cdot{\rm s/g}$, $A_{\rm GM}(1.9) = 47.2\,{\rm cm}\cdot{\rm s/g}$.

4 Conclusions

We have studied the back-reaction of the quantum vortex tangle on the mean laminar normal velocity profile in the channel counterflow. The initially parabolic V_n evolves to a flatter shape. The vortex tangle influences the mean normal velocity profile via the mutual friction force. As a result, the global properties of the flow change compared to the uncoupled dynamics, with effect being stronger for high temperatures and counterflow velocities. At low and moderate temperatures, the flow and tangle properties are close to those with the time-independent normal velocity profile. We propose a model of $V_{\rm n}(y)$, expressed via $\langle V_{\rm n}\rangle$, that accounts for the effect of the mutual friction.

Acknowledgements We acknowledge useful and encouraging discussions with V. L'vov and I. Procaccia.

References

1. C.F. Barenghi, L. Skrbek, K.R. Sreenivasan, Proc. Natl. Acad. Sci. USA **111**, 4647 (2014)
2. W.F. Vinen, J.J. Niemela, J. Low Temp. Phys. **128**, 167 (2002)
3. L. Skrbek, K.R. Sreenivasan, Phys. Fluids **24**, 011301 (2012)
4. R.J. Donnelly, *Quantized Vortices in Helium II* (Cambridge Univ, Press, 1991)
5. C.F. Barenghi, R.J. Donnelly, W.F. Vinen (ed.), *Quantized Vortex Dynamics and Superfluid Turbulence*, vol. 571, Lecture Notes in Physics (Springer, Berlin, 2001)
6. H.E. Hall, W.F. Vinen, Proc. R. Soc. Lond. A Math. Phys. Sci. **238**, 215 (1956)

7. I.L. Bekarevich, I.M. Khalatnikov, Sov. Phys. JETP **13**, 643 (1961)
8. K.W. Schwarz, Phys. Rev. B **31**, 5782 (1985)
9. K.W. Schwarz, Phys. Rev. B **38**, 2398 (1988)
10. C. Barenghi, D.C. Samuels, Phys. Rev. B **60**, 1252 (1999)
11. O.C. Idowu, D. Kivotides, C.F. Barenghi, D.C. Samuels, J. Low Temp. Phys. **120**, 269 (2000)
12. D. Kivotides, C.F. Barenghi, D.C. Samuels, Science **290**, 777 (2000)
13. D.C. Samuels, Phys. Rev. B **46**, 11714 (1992)
14. R.G.K.M. Aarts, A.T.A.M. de Waele, Phys. Rev. B **50**, 10069 (1994)
15. A.W. Baggaley, S. Laizet, Phys. Fluids **25**, 115101 (2013)
16. A.W. Baggaley, J. Laurie, J. Low Temp. Phys. **178**, 35 (2015)
17. S. Yui, M. Tsubota, Phys. Rev. B **91**, 184504 (2015)
18. D. Khomenko, L. Kondaurova, V.S. L'vov, P. Mishra, A. Pomyalov, I. Procaccia, Phys. Rev. B **91**, 180504(R) (2015)
19. J.T. Tough, in *Progress in Low Temperature Physics*, Vol. VIII. Chap 3, ed. by D.F. Brewer (North-Holland, Amsterdam, 1982)
20. L. Galantucci, M. Sciacca, C.F. Barenghi, Phys. Rev. B **92**, 174530 (2015)
21. L. Kondaurova, V.S. L'vov, A. Pomyalov, I. Procaccia, Phys. Rev. B **89**, 014502 (2014)
22. A.W. Baggaley, C. Barenghi, Phys. Rev. B **83**, 134509 (2011)
23. L. Gamet, F. Ducros, F. Nicoud, T. Poinsot, Int. J. Numer. Methods Fluids **29**, 2 (1999)
24. R.J. Donnelly, C.F. Barenghi, J. Phys. Chem. Ref. Data **27**, 6 (1998)
25. A. Marakov, J. Gao, W. Guo, S.W. Van Sciver, G.G. Ihas, D.N. McKinsey, W.F. Vinen, Phys. Rev. B **91**, 094503 (2015)
26. D. Khomenko, V.S. Lvov, A. Pomyalov, I. Procaccia, Phys. Rev. B **93**, 134504 (2016)
27. C.J. Gorter, J.H. Mellink, Physica **15**, 285 (1945)